Advanced Steel Construction – Vol. 18 No. 1 (2022) 488–494
DOI:10.18057/IJASC.2022.18.1.7

TENSILE BEHAVIOUR OF TMCP Q690D HIGH-STRENGTH STRUCTURAL STEEL AT STRAIN RATES FROM 0.00025 TO 760 S^{-1}

Jing-Si Huo [1,*], Xiang Zeng [2] and Hai-Tao Wang [3]

[1] *College of Civil Engineering, Huaqiao University, Xiamen, 361021, China*
[2] *College of Civil Engineering and Architecture, Hainan University, Haikou, 570228, China*
[3] *College of Civil Engineering, Hunan University, Changsha, 410082, China*
** (Corresponding author: E-mail: jingsihuo@gmail.com)*

ABSTRACT

The application of Q690D high-strength structural steel (HSSS) has been increasing in engineering structures. The lack of knowledge of the strain rate behaviour limits the application to the extreme loading conditions such as blast and impact loadings. This paper presents a series of tensile tests on the dynamic tensile behaviour of Q690D HSSS produced through the thermo-mechanical control process (TMCP). The stress-strain relationships of TMCP Q690D in the strain rate range of 0.00025 to 760 s^{-1} were measured by using the universal and servo-hydraulic high speed testing machines. The experimental results verified the sensitivity to strain rate of TMCP Q690D and the dynamic increase factor (DIF) for yield stress is identical to that of QT (Quenched and Tempered) S690 HSSS. However, TMCP Q690D behaves in a much different way in the strain hardening stage. The commonly-used Cowper-Symonds model was calibrated for the DIFs of yield stress and ultimate tensile strength. The Johnson-Cook (J-C) model was modified and a new rate-dependent constitutive model was proposed. The proposed model was validated successfully to predict the true stress-strain relationship, providing better prediction results than the modified J-C model.

ARTICLE HISTORY

Received: 16 October 2020
Revised: 1 June 2021
Accepted: 5 June 2021

KEYWORDS

TMCP Q690D steel;
Strain rate effect;
Dynamic tensile test;
Dynamic increase factor;
Rate-dependent constitutive model

1. Introduction

The mechanical behaviour of steel had been proved to be sensitive to strain rate [1-2], which mainly manifests with the increase of the yield and ultimate tensile strengths and the variation of strain hardening with the strain rate. Structural steel is a typical rate-dependent material and the strain-rate effect significantly influences the dynamic behaviour of steel structures under impact and explosion [3-4], even the strong earthquake action [5]. Thus, the rate-dependent behaviour is vital to evaluate the performance of steel and steel-concrete composite structures subjected to the accidental loads.

The utilisation of high-strength structural steel (HSSS) in engineering structures has been increasing due to its many advantages [6]. The 690 MPa grade HSSS, which has been developed in different countries [7-10], has been used in buildings, bridges, and towers [11-12] as well as offshore structures [13-14]. To promote the application of 690 MPa grade HSSS to the engineering structures subjected to dynamic loading conditions, it is of significance to investigate the strain rate-dependent behaviour.

The strain rate-dependent behaviours of structural steel of different grades with the yield strength ranging from 321 to 906 MPa have been investigated [15-23]. The existing references show that structural steel is sensitive to strain rate and its yield stress is more sensitive to strain rate than the ultimate tensile strength. The post-yielding behaviour is significantly different from that at a static loading condition. For the strain rate-dependent mechanical behaviour of 690 MPa grade HSSS, the efforts have been made to investigate quenched and tempered (QT) HSSS S690 in the past three years [15-17]. Alabi et al. [15] pointed out that more test data is imperative to validate the reliable strain rate effect on the QT S690QL and S960QL HSSS at strain rates from 4 to 100 s^{-1}. Yang et al. [16-17] examined the tensile behaviour of QT S690 at the wider strain rates from 0.00025 to 4109 s^{-1} and provided the model of dynamic increase factor (DIF) for yield stress and constitutive model.

Although the yield stress has a certain degree of influence on the strain rate effect, there is still under discussion on the relationship between yield stress and strain-rate behaviour [17]. Furthermore, Alabi et al. [15] concluded that the sensitivity to strain rate is affected by the chemical compositions, production routes, and microstructure. Especially, the thermo-mechanical control process (TMCP) and QT process are the two important ways to improve the strength of steel from the point of metallurgy. For TMCP steel, the high strength and comprehensive properties result from the mechanism of grain refinement, precipitation strengthening, or phase-transformation strengthening. The strengthening mechanism is realized by combining controlled rolling and controlled cooling methods. For QT steel, the high strength stems from the tempered martensite microstructure which forms after reheating, quenching, and further tempering heat treatment of hot-rolled steel. The tempering process for QT steel aims to improve the toughness of martensite (being high strength and brittle) produced in the quenching process and to balance the strength and toughness of steel. Even though QT and TMCP steels have the similar chemical compositions, there are differences in grain size and microstructure between them, and therefore, QT and TMCP steels behave in different mechanical properties [24]. The strain rate-dependent behaviour of 690-MPa QT steel (S690) has been investigated, but the strain rate-dependent behaviour of 690-MPa TMCP steel still needs to be clarified.

The present paper aims to study the mechanical behaviour of TCMP Q690D HSSS at different strain rates. A series of tensile tests were conducted to obtain the stress-strain curves within the strain rate range from 0.00025 to 760 s^{-1}. A comparison of the strain-rate behaviour between TCMP Q690D and QT S690 reported in previous studies was performed. According to the measured results, the models for the DIFs for yield and tensile strengths as well as the rate-dependent constitutive model of TCMP Q690D are discussed and proposed.

2. Experimental programme

2.1. Specimens preparation

TMCP Q690D HSSS was used in the tests. Table 1 summarizes the chemical composition and carbon equivalent value (CEV), which meet the requirements of Standard GB/T 1591-2008 [7].

The geometry of all specimens was determined according to the Standard ISO 26203-2:2011 [25]. The thickness of the specimen is 3 mm and the width over the parallel length is 6 mm. As shown in Fig. 1, the parallel length and gauge length are 15 mm and 12 mm, respectively.

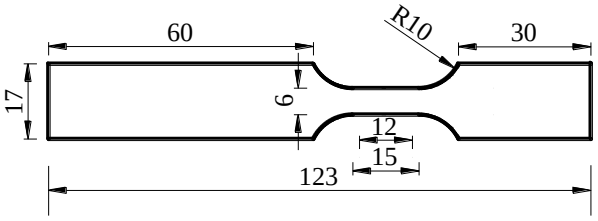

Fig. 1 Specimen geometry (unit: mm)

2.2. Test setup and instrumentation

Different test methods were used for the tension tests. A universal electromechanical machine walter+bai ag (LFM- TOP 50 kN) was used to produce the strain rates of 0.00025 and 0.002 s^{-1}. The tension tests with a wide

range of strain rates (from 0.1 to 760 s^{-1}) were conducted by means of a servo-hydraulic high-speed testing machine (Fig. 2) which has been used by other researchers [17, 20, 21, 26, 27]. The tested results at the strain rate of 0.00025 s^{-1} can be taken as the quasi-static properties [28-29].

As shown in Fig. 2, the dynamic tension was activated by the movement of the upper accelerated grip, which was fixed to the hydraulic actuator. A piezoelectric force cell was installed inside of the fixed grip to measure the dynamic tensile force when the strain rate is lower than 100 s^{-1}. Due to the limitation of the frequency response of the piezoelectric force cell, two strain gauges were mounted onto the lower end of the specimen to determine the tension force at strain rates above 100 s^{-1}. Meanwhile, the measurement of the strain in the gauge length was realized through the 3D non-contact deformation measurement system [26] which is equipped with a high speed video camera, image acquisition software, and digital image correlation software.

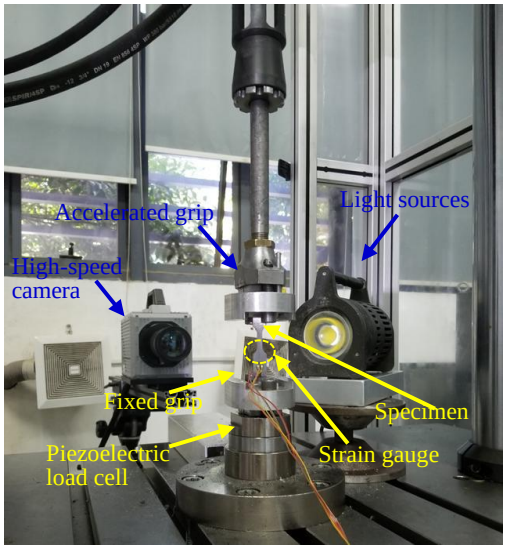

Fig. 2 Setup of high-speed tensile test

3. Results and discussion

3.1. Engineering stress-strain curves at various strain rates

Fig. 3 shows the engineering stress-strain curves at strain rates ranging from 0.00025 to 763 s^{-1}. The measured curves of repeated specimens at different strain rates have good consistency and repeatability, which demonstrates the reliability of the test data. The curves with oscillation were processed, and the processed curves keep in consistency with the original ones. The average curve of the three repeated stress-strain curves at each strain rate was taken as the representative curve (indicated by the green line in Fig. 3), which was used for the following analysis.

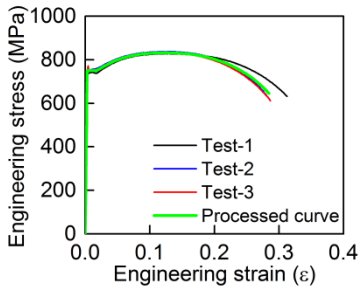

(a) 0.00025 s^{-1} (Quasi-static)

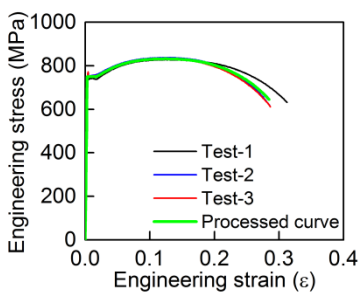

(b) 0.002 s^{-1}

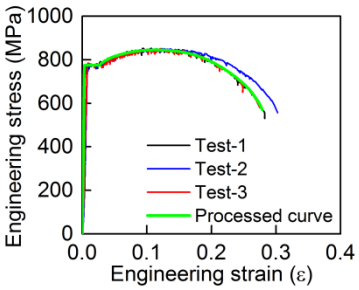

(c) 0.08 s^{-1}

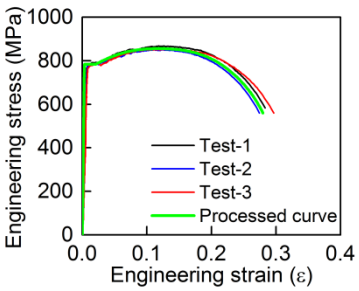

(d) 0.99 s^{-1}

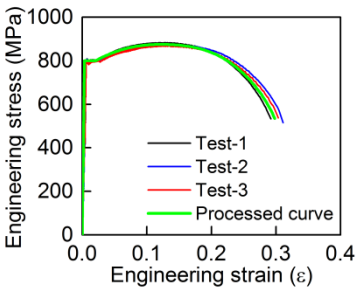

(e) 7.9 s^{-1}

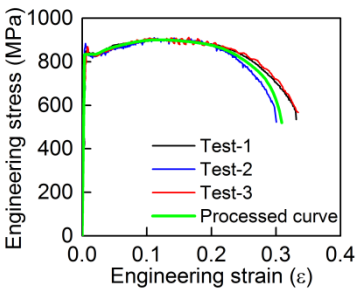

(f) 75.6 s^{-1}

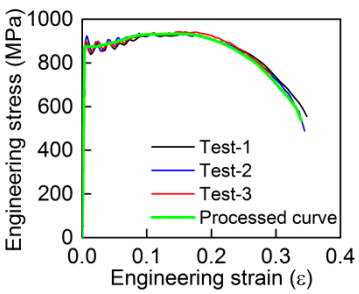

(g) 466 s^{-1}

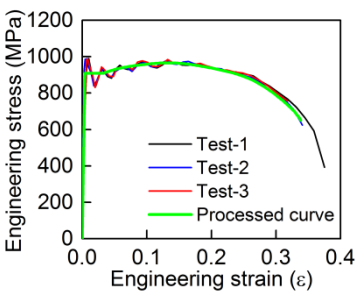

(h) 763 s^{-1}

Fig. 3 Raw and processed engineering stress-strain curves of TMCP Q690D

Fig. 4 compares the stress-strain curves of TMCP Q690D at different strain rates. It can be observed that the increase in strain rate results in the increased yield and tensile strengths. The yield plateau can be seen in all curves (Fig. 3 and Fig. 4) and its length increases with the strain rate. The phenomenon is similar to that of QT S690 at different strain rates [16-17].

The yield strength (f_y), ultimate tensile strength (f_u), and uniform elongation (ε_u) of TMCP Q690D steel at various strain rates are summarized in Table 2. The dynamic increase factors for the three mechanical indexes, abbreviated as DIF_y, DIF_u, and $DIF_{\varepsilon u}$ respectively, are also given in Table 2. Conventionally, the DIF for a mechanical index is expressed as the ratio of its dynamic value to its quasi-static value. The table shows that the raising of strain rate leads to the increased yield and tensile strengths. When the strain rate increases from 0.00025 to 763 s^{-1}, yield strength and tensile strength increase obviously, from 724 to 908 MPa (increased by 25.4%) and from 812 to 968 MPa (increased by 19.2%), respectively. The sensitivity to strain rate of the yield strength is more significant than that of the tensile strength. However, the uniform elongation does not change in a monotonic manner with the strain rate increasing, which is similar to Q420 steel [21]. The uniform elongation is between 11% and 15% and the corresponding $DIF_{\varepsilon u}$ is between 0.904 and 1.173 at different strain rates.

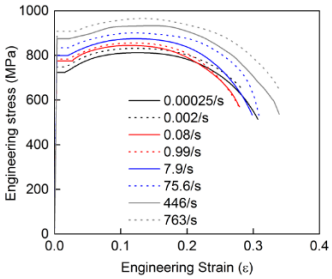

Fig. 4 Stress-strain curves of TMCP Q690D at various strain rates

Table 1
Chemical composition and CEV of TMCP Q690D (in weight %)

Element	C	Si	Mn	P	S	Nb	V	Ti	Cr	Cu	Mo	Ni	B	CEV
%	0.07	0.09	1.5	0.013	0.003	0.046	0.003	0.099	0.02	0.013	0.01	0.02	0.0001	0.329

Table 2
Mechanical properties of TMCP Q690D steel at various strain rates

Strain rate (s^{-1})	Yield stress (MPa)	Ultimate tensile strength (MPa)	Uniform elongation ε_u	DIF_y	DIF_u	$DIF_{\varepsilon u}$
0.00025	724	812	0.1255	1.000	1.000	1.000
0.002	749	831	0.12561	1.035	1.023	1.001
0.08	775	845	0.11345	1.070	1.041	0.904
0.99	784	855	0.11796	1.083	1.053	0.940
7.9	799	875	0.12362	1.104	1.078	0.985
75.6	834	903	0.12084	1.152	1.112	0.963
446	875	933	0.14719	1.209	1.149	1.173
763	908	968	0.13249	1.254	1.192	1.056

3.2. Models for DIF_y and DIF_u

In order to clarify the difference of DIF_y and DIF_u between TMCP Q690D and QT S690 steel, Fig.5 illustrates a comparison of the test results from the present experiment and References [16-17]. In addition, the quasi-static strain rate is set as 0.00025 s^{-1}. Fig. 5 depicts that the DIF_y versus strain rate curves of TMCP Q690D are identical to those of QT S690, and the DIF_u of QT S690 steel is also identical to the corresponding DIF_y at the same strain rate. The DIF_u of TMCP Q690D is fairly lower than that of QT S690.

C-S model proposed by Cowper and Symonds in 1957 [30] had been widely used to predict the DIF of the strength of steel and is expressed as

$$DIF_y = 1 + \left(\frac{\dot{\varepsilon}}{D}\right)^{\frac{1}{q}} \quad (1)$$

where $\dot{\varepsilon}$ stands for the strain rate, D and q are material constants which can be calibrated by the test data. Yang et al. [16-17] calibrated the parameters

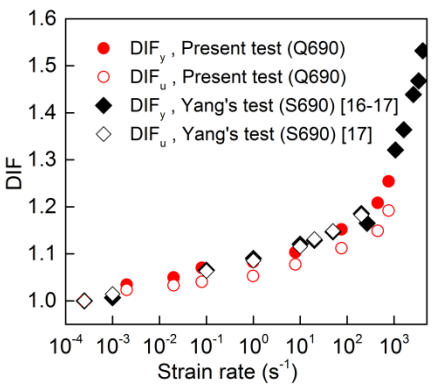

Fig. 5 Comparison of DIF_y and DIF_u between TMCP Q690D and QT S690

of the C-S model for the DIF_y and DIF_u of QT S690 at different strain rate ranges (seen in Table 3). The model is adopted for the comparison with the test results of TMCP Q690D, as shown in Fig. 6 and Fig. 7. Fig. 6 shows that the C-S model [17], which is calibrated based on the measured results of QT S690 when $\dot{\varepsilon} \leq 200$ s^{-1}, underestimates the DIF_y seriously at larger strain rates. The calibrated C-S model [16] based on the test results of QT S690 at $\dot{\varepsilon}$ from 266 to 4109 s^{-1} underestimates the DIF_y at lower strain rates. Thus, the existing C-S model for DIF_y of QT S690 can not exactly describe the DIF_y in the entire strain rate range. Combining the DIF_y test data of TMCP Q690D with that of QT S690, an attempt to calibrate the C-S model is made to predict the DIF_y exactly over the entire test strain rate range. But it is found that the C-S model is not suitable in the entire strain rate range. In Fig. 6, it is observed that there exists a distinct turning point in the DIF_y versus strain rate curves. Therefore, a modified C-S model based on a piecewise function is proposed for the DIF_y. Through fitting the DIF_y test data of TMCP Q690D and QT S690, the parameters of C-S model for them are obtained, as shown in Table 4. When $\dot{\varepsilon} \leq 264$ s^{-1}, $D = 1.141 \times 10^8$ s^{-1} and q=7.57. And when $\dot{\varepsilon} > 264$, D=22946 s^{-1} and q=2.6. The comparison between the modified C-S model and test results shown in Fig. 6 demonstrates that the modified model provides an excellent prediction accuracy for their DIF_y.

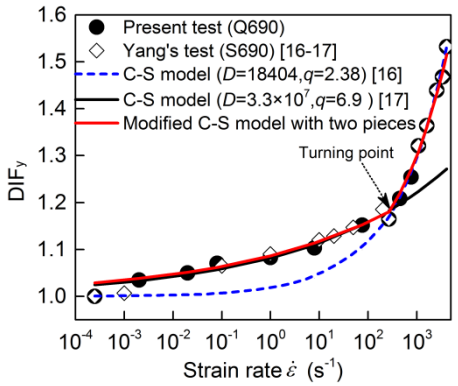

Fig. 6 Predicted DIF_y at strain rates from 0.00025 to 4109 s^{-1} in comparison with test results

Fig. 7 presents the comparison of DIF_u between the existing models and experimental results. The Malvar model was presented according to the experimental results of steel reinforcing bars with yield stresses between 290 and 710 MPa and with strain rates between 10^{-4} and 10 s^{-1} [1]. As shown in Fig. 7, the margin of error is not acceptable for the predicted DIF_u based on the malvar model with a linear formula. The C-S model of DIF_u for QT S690 (Table 3) [17] overestimates the DIF_u of TMCP Q690D. Therefore, the parameters in C-S model of DIF_u for TMCP Q690D are recalibrated with D=5.9×10^7 and q=6.33 (summarized in Table 4). Fig. 7 shows that the recalibrated C-S model provides good predicted results of DIF_u of TMPC Q690D.

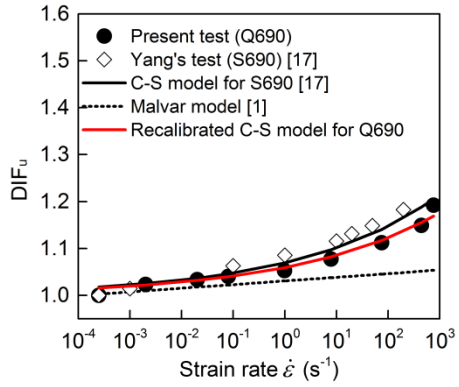

Fig. 7 Comparison of DIF_u from models and test results

Table 3
C-S models for DIF_y and DIF_u of QT S690

Test	Strain rate (s^{-1})	Parameters for DIF_y		Parameters for DIF_u	
		D (s^{-1})	q	D (s^{-1})	q
SHPB Test [16]	0.00025, 266 to 4109	18404	2.38	-	-
Tension test [17]	0.001 to 200	3.3×10^7	6.9	1.2×10^7	6.1

Table 4
Calibrated parameters of C-S model for TMCP Q690D

Strain rate (s^{-1})	Parameters for DIF_y		Parameters for DIF_u	
	D (s^{-1})	q	D (s^{-1})	q
≤264	1.141×10^8	7.57	5.9×10^7	6.33
>264	22946	2.6		

3.3. Rate-dependent constitutive laws for TMCP Q690D steel

When steel or composite structures subjected to high dynamic loads are evaluated using an explicit nonlinear dynamic finite element procedure, the true rate-dependent mechanical properties of steel are required. In order to simulate the true mechanical properties, a rate-dependent constitutive model is usually developed based on the measured stress-strain curves.

3.3.1. J-C model

J-C model proposed by Johnson and Cook in 1983 [31] is widely applied to simulate the true stress-strain constitutive behaviour of steel in the nonlinear finite element simulations of dynamic cases. The flow stress (σ) can be expressed as

$$\sigma = \left[A + B(\varepsilon_p)^n\right]\left[1 + C\ln(\frac{\dot{\varepsilon}}{\dot{\varepsilon}_0})\right](1 - T^{*m}) \quad (2)$$

where $\dot{\varepsilon}$ is the strain rate, ε_p is the plastic strain, $\dot{\varepsilon}_0$ is the reference strain rate. Here, $\dot{\varepsilon}_0$ is taken as the quasi-static strain rate 0.00025 s^{-1}. T^* is the homologous temperature. The material constants include A, B, C, n, and m. Eq. 2 contains the strain hardening effect under quasi-static load (denoted by the first bracket), strain-rate, and thermal softening effects on the strain hardening behaviour (described by the second bracket and third bracket, respectively). The thermal softening effect described by the third bracket is for the metal materials under high temperatures. The present test is performed at room temperature and thus the thermal softening effect is not considered in the constitutive model and the value of the third bracket is taken as 1. Then, Eq. 2 can be simplified into Eq. 3,

$$\sigma = \left[A + B(\varepsilon_p)^n\right]\left[1 + C\ln(\frac{\dot{\varepsilon}}{\dot{\varepsilon}_0})\right] \quad (3)$$

Heat is generated in specimens when plastic deformation occurs, and the adiabatic heating effect at a high strain rate will increase the temperature in the specimens, but for simplicity, the temperature effect is generally considered to be contained in the effect of strain rate, namely, the stress-strain curves described by Eq. 3 automatically considers the increase of temperature due to the adiabatic heating effect.

Eq. 3 has been used to describe the constitutive behaviour of QT S690 steel [16-17] and the coefficients A, B, C, and n in the equation were calibrated and modified by fitting the test results. The values of those coefficients in Eq. 3 are listed in Table 5. Furtherly, a modified J-C model (Eq. 4) with $(1 + J\dot{\varepsilon}^K)$ instead of $(1 + C\ln(\dot{\varepsilon}/\dot{\varepsilon}_0))$ for the strain rate effect (denoted by S690-M-J-C model hereafter) [17] was proposed for describing the constitutive behaviour at the strain rates ranging from 0.001 to 4109 s^{-1} (Table 5).

$$\sigma = [A + B(\varepsilon_p)^n](1 + J\dot{\varepsilon}^K) \quad (4)$$

To discover whether the constitutive model of QT S690 steel [17] is able to describe the constitutive behaviour of TMCP Q690D steel, a comparison between the S690-M-J-C model and the test results of TMCP Q690D is performed, as shown in Fig. 8. The figure shows that the true stress-strain curves predicted by the S690-M-J-C model are quite different from the test curves of TMCP Q690D. S690-M-J-C model has been demonstrated to be well consistent with the test curves of QT S690. Therefore, the comparison indicates that TMCP Q690D and QT S690 have different strain hardening behaviour.

The strain rate term of the standard J-C model is linear in the logarithm of the strain rate (Eq.2). The linear strain rate term is not always suitable for describing the effect of strain rate on the true stress-strain curve of any mental, and thus it can be modified into other forms such as the exponential forms in strain rate [16-17, 32] and the quadratic form in the logarithm of the strain rate [33]. To accurately predict the true stress-strain curves of TMCP Q690D, the J-C models should be recalibrated or modified to acquire the appropriate quasi-static strain hardening term and strain rate term. The coefficients A, B, and n in the model can be obtained through fitting the quasi-static true stress-strain curve with the power function $(A + B(\varepsilon_p)^n)$ in Eq. 3.

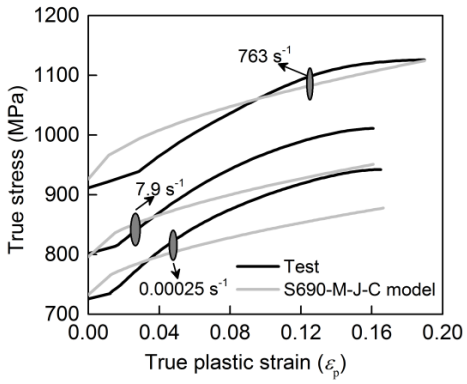

(a)

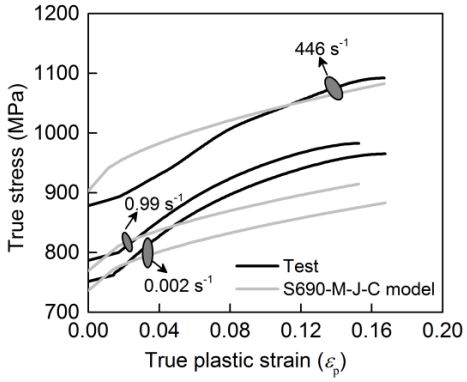

(b)

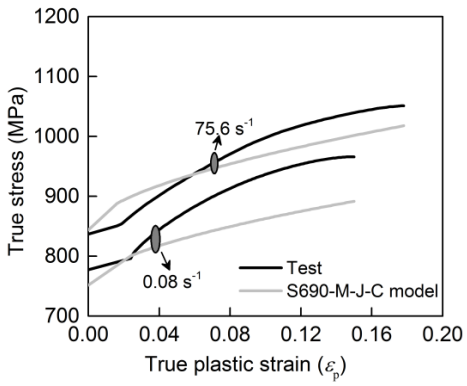

(c)

Fig. 8 Comparison between S690-M-J-C model and test results of TMCP Q690D

Table 5
J-C model for true stress-strain curve of QT S690

J-C Model	Strain rate /s^{-1}	*A* (MPa)	*B* (Mpa)	*n*	*C*	*J*	*K*
Eq. (3)	0.00025, 266 to 4109[16]	722	400	0.57	$0.0041\dot{\varepsilon}^{0.217}$	-	-
	0.001 to 200 [17]	727	400	0.57	0.012	-	-
Eq. (4)	0.001 to 4109 [17]	727	400	0.57	-	0.06	0.23

Fig. 9 illustrates the ratio of true stress-strain curves at different strain rates to the curve at quasi-static strain rate in the whole strain range. In other words, it presents the strain rate term of the J-C model for TMCP Q690D at different strain, which is denoted by $\mathrm{DIF}(\dot{\varepsilon},\varepsilon_p)$ in Fig. 9. The $\mathrm{DIF}(\dot{\varepsilon},\varepsilon_p)$ of the curves are different at different strain, especially for those at high strain rates. Therefore, an average of $\mathrm{DIF}(\dot{\varepsilon},\varepsilon_p)$ ($\mathrm{DIF_{ave}}$) for each strain rate is used to alleviate the difference of $\mathrm{DIF}(\dot{\varepsilon},\varepsilon_p)$ in the entire strain range. The $\mathrm{DIF_{ave}}$ is shown in Fig. 9 and can be fitted with an exponential form in $\dot{\varepsilon}$ $(1+0.0564\dot{\varepsilon}^{0.1803})$, as shown in Fig. 10. Hence, the modified J-C model for TMCP Q690D is described as Eq. 4 with J=0.0564 and K=0.1803. Table 6 summarizes all the coefficients in the modified J-C model for TMCP Q690D. A comparison between the modified J-C model and test results is made in Fig. 11. The figure shows the modified J-C model provides better-predicted results than the S690-M-J-C model shown in Fig. 8.

Table 6
Modified J-C model for TMCP Q690D

Modified J-C Model	*A* (MPa)	*B* (MPa)	*n*	*J*	*K*
Eq. (4)	f_y	873	0.7272	0.0564	0.1803

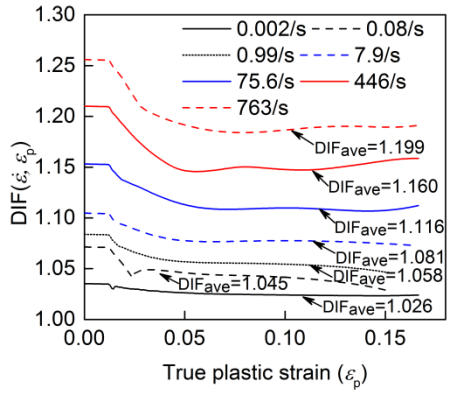

Fig. 9 $\mathrm{DIF_{ave}}$ at various strain rates

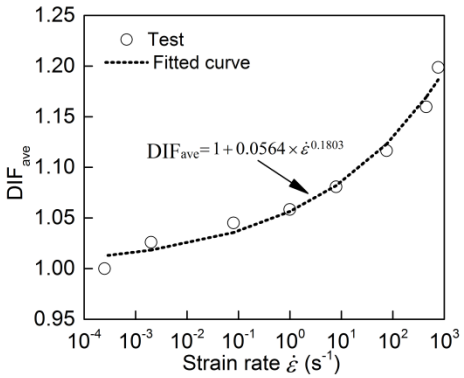

Fig. 10 Fitting $\mathrm{DIF_{ave}}$

3.3.2. Proposed constitutive model

A new constitutive model is necessary to forecast the true stress-strain curve of TMCP Q690D at different strain rates more precisely. From Fig. 4 and Fig. 11, it can be observed that the stress-strain curves at different strain rates are approximately parallel, namely, the strain hardening rate of the curves is approximately consistent in the entire plastic strain range. Hence, the true stress-strain curve can be expressed as Eq. (5) [34].

$$\sigma = \sigma_0(\dot{\varepsilon}) + \alpha(\varepsilon_p) = \sigma_s M(\dot{\varepsilon}) + \alpha(\varepsilon_p) \tag{5}$$

where $\alpha(\varepsilon_p)$ represents the consistent strain hardening curve at different strain rates and $\sigma_0(\dot{\varepsilon})$ means the stress at the initiation of the curve at a strain rate $\dot{\varepsilon}$. The $\alpha(\varepsilon_p)$ can be obtained by subtracting the quasi-static yield stress from the quasi-static curve. Fig. 12 illustrates Eq. (5), namely, the true stress-strain curve at the strain rate $\dot{\varepsilon}$ can be obtained by translating the $\alpha(\varepsilon_p)$ with a distance of $\sigma_0(\dot{\varepsilon})$ upwards. Furtherly, the $\sigma_0(\dot{\varepsilon})$ can be expressed by the product of σ_s and $M(\dot{\varepsilon})$, where the σ_s means the quasi-static yield stress and the $M(\dot{\varepsilon})$ represents the strain rate effect.

The $\alpha(\varepsilon_p)$ can be expressed by Eq. (6) with El-Magd quasi-static flow model [35] for reference.

$$\alpha(\varepsilon_p) = A_1\varepsilon_p + B_1(1 - exp(-\beta\varepsilon_p)) \tag{6}$$

where A_1, B_1, and β are material constants. A_1, B_1, and β are acquired by fitting the quasi-static test results, which are listed in Table 7. Fig. 11(a) shows that Eq. 6 is more suitable for the quasi-static strain hardening curve of TMCP Q690D than is the exponential expression ($A+B(\varepsilon_p)^n$) in the J-C model.

Table 7
Coefficients in Eq. (6)

Parameters	A_1 (MPa)	B_1 (MPa)	β
Value	-8741	9707	1.139

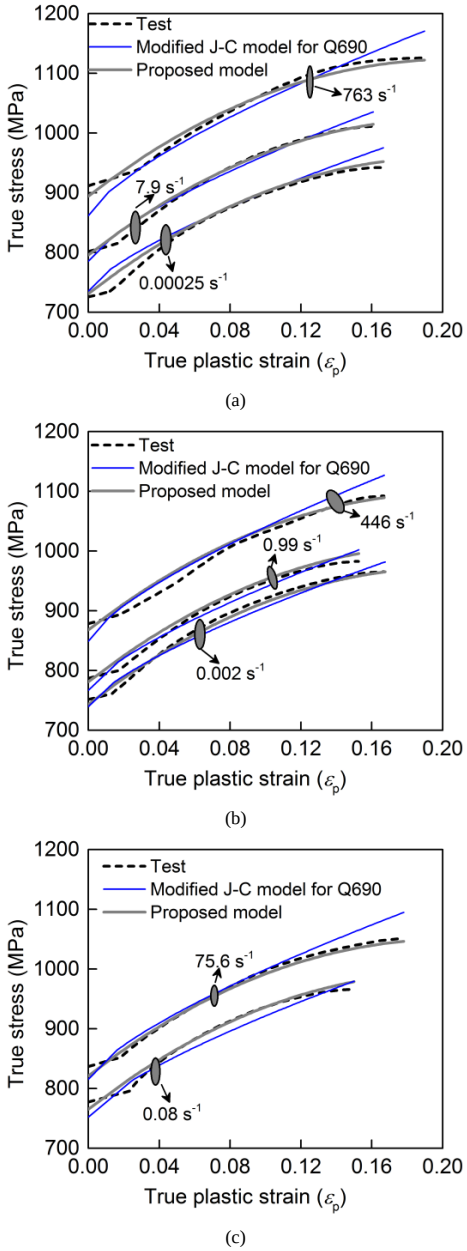

Fig. 11 Comparison between Modified J-C model, proposed model, and test results of TMCP Q690D

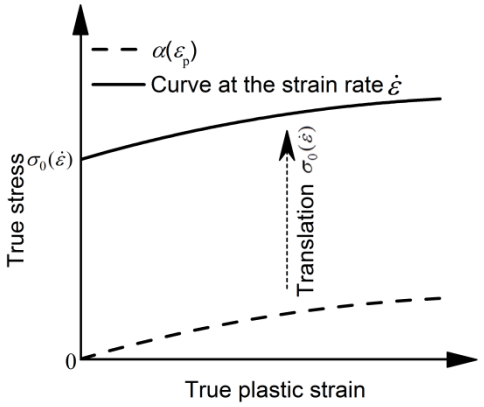

Fig. 12 Relationship between the true stress-strain curve and $\alpha(\varepsilon_p)$

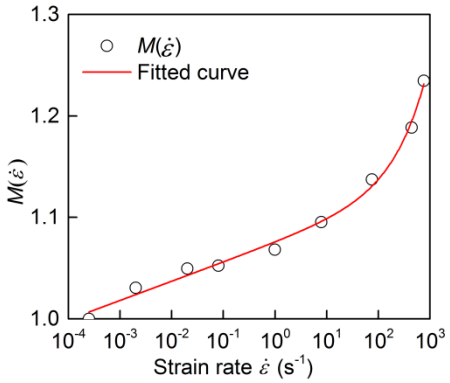

Fig. 14 Fitting $M(\dot{\varepsilon})$

Fig. 13 depicts the true stress difference ($\Delta\sigma(\dot{\varepsilon},\varepsilon_p)$) between dynamic and quasi-static curves at the same plastic strain. It is observed from Fig. 13 that the $\Delta\sigma(\dot{\varepsilon},\varepsilon_p)$ is not a constant for every dynamic curve, which indicates that the true stress-strain curves are not strictly parallel. So, an average of $\Delta\sigma(\dot{\varepsilon},\varepsilon_p)$ ($\Delta\sigma_{ave}(\dot{\varepsilon})$) is used, which is suitable to represent the $\Delta\sigma(\dot{\varepsilon},\varepsilon_p)$ in the entire plastic strain range. The $\Delta\sigma_{ave}(\dot{\varepsilon})$ is calculated and given in Fig. 13. Then, $\sigma_0(\dot{\varepsilon})$ in Eq. 5 can be express as ($\sigma_s+\Delta\sigma_{ave}(\dot{\varepsilon})$) and $M(\dot{\varepsilon})$ is expressed as

$$M(\dot{\varepsilon})=\frac{\sigma_0(\dot{\varepsilon})}{\sigma_s}=1+\frac{\Delta\sigma_{ave}(\dot{\varepsilon})}{\sigma_s} \tag{7}$$

Introducing the σ_s from test and $\Delta\sigma_{ave}(\dot{\varepsilon})$ shown in Fig. 13 into the Eq. (7), and the value of $M(\dot{\varepsilon})$ can be computed, which is depicted in Fig. 14. Through fitting $M(\dot{\varepsilon})$ with the data in Fig. 14, an expression for $M(\dot{\varepsilon})$ is obtained as Eq. 8.

$$M(\dot{\varepsilon})=1.007+(\dot{\varepsilon}/20106)^{1/1.4336}+0.00821\ln(\dot{\varepsilon}/\dot{\varepsilon}_0) \tag{8}$$

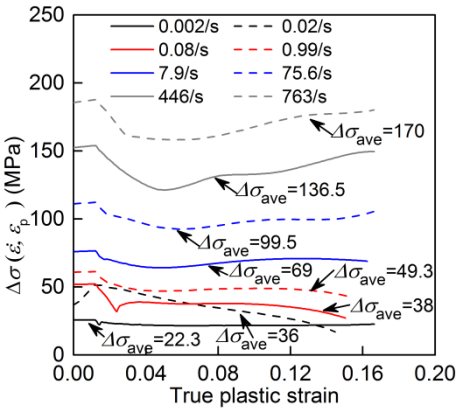

Fig. 13 Difference of true stress ($\Delta\sigma(\dot{\varepsilon},\varepsilon_p)$) between dynamic and quasi-static curves

Fig. 11 shows a comparison among the proposed model (Eqs. 5-8), modified J-C model, and the test results. The comparison demonstrates that the proposed model predicts the true stress-strain curves with good accuracy within the range of strain rates from 0.00025 to 760 $s^{-1}$and it is much better for TMCP Q690D than the modified J-C model.

4. Conclusions

In this paper, the dynamic behaviour of TMCP Q690D steel at different strain rates (from 0.00025 to 760 s^{-1}) has been tested and stress-strain curves were measured. Based on the experimental and analytical results, the conclusions can be obtained as follows:

(1) The strain-rate sensitivity of yield stress of TMCP Q690D steel is exactly similar to that of QT S690 steel. The strain-rate sensitivity of tensile strength of TMCP Q690D steel is fairly lower than that of QT S690 steel. The strain hardening response of TMCP Q690D steel at different strain rates are very different from those of QT S690 steel, which behaves in the way that the strain hardening rate of TMCP Q690D steel is higher than that of QT S690 steel.

(2) Based on the test data of TMCP Q690D and QT S690, the material constants in the C-S model for two different strain rate ranges (≤264 s^{-1} and >264 s^{-1}) are exactly calibrated to predict the DIF_y. Moreover, the C-S model employed to represent the DIF for tensile strength of TMCP Q690D is calibrated.

(3) The existing J-C model for QT S690 is not suitable to simulate the true stress-strain relationship of TMCP Q690D. The modified J-C model based on the test results of TMCP Q690D provides a better prediction than the J-C model for QT S690 does.

(4) A newly proposed constitutive model can predict the true stress-strain curves of TMCP Q690D with higher accuracy than the modified J-C model.

Acknowledgments

The authors gratefully acknowledge the support provided by the National Natural Science Foundation of China (51678256, 51438010, and 51608156).

References

[1] Malvar L.J., “Review of static and dynamic properties of steel reinforcing bars”, ACI Materials Journal, 95, 609-616, 1998.
[2] Ritchie C.B., Packer J.A., Zhao X.L., Heidarpour A. and Chen Y.Y., “Dynamic material performance of cold-formed steel hollow sections: a state-of-the-art review”, Frontiers of Structural and Civil Engineering, 11, 209-227, 2017.
[3] Ribeiro J., Santiago A., Rigueiro C., Barata P. and Veljkovic M., “Numerical assessment of T-stub component subjected to impact loading”, Engineering Structures, 106,450-460, 2016.
[4] Liew J.Y.R., “Survivability of steel frame structures subject to blast and fire”, Journal of Constructional Steel Research, 64, 854-866, 2008.
[5] Lamarche C.P. and Tremblay R., “Seismically induced cyclic buckling of steel columns including residual-stress and strain-rate effects”, Journal of Constructional Steel Research, 67, 1401-1410, 2011.
[6] Li G.Q., Wang Y.B. and Chen S.W., “The art of application of high-strength steel structures for buildings in seismic zones”, Advanced Steel Construction, 11, 492-506, 2015.
[7] GB/T 1591-2008, High strength low alloy structural steels, Standards Press of China, Being, 2009. (in Chinese).
[8] GB/T 16270-2009, High strength structural steel plates in the quenched and tempered condition, Standards Press of China, Being, 2010. (in Chinese).
[9] BS EN 10025–6: 2004, Hot rolled products of structural steels - Part 6: Technical delivery conditions for flat products of high yield strength structural steels in the quenched and tempered condition, British Standards, 2004.
[10] ASTM A514/A514M-00a, Standard specification for high-yield-strength, quenched and tempered alloy steel plate, suitable for welding, American Society for Testing and Materials, West Conshohocken, PA, 2000.
[11] Shi G., Hu F.X. and Shi Y.J., “Recent research advances of high strength steel structures and codification of design specification in china”, International Journal of Steel Structures, 14, 873-887, 2014.
[12] Schröter F. and Lehnert T., “Trends in the application of high-performance steel in european bridge building”, In: Petzek E., Bancila R. (eds), The Eight International Conference "Bridges in Danube Basin", Springer Vieweg, Wiesbaden, 2014.
[13] Chiew S.P., Zhao M.S. and Lee C.K., “Mechanical properties of heat-treated high strength steel under fire/post-fire conditions”, Journal of Constructional Steel Research, 98, 12-19, 2014.
[14] Wang Y., MacDonald A., Xu L., Wright M. and Shenoi R.A., “Engineering critical assessment and variable sensitivity analysis for as-welded S690 steels”, Engineering Failure Analysis, 109, 104282, 2020.
[15] Alabi A.A., Moore P.L., Wrobel L.C. and He W., “Tensile behaviour of S690QL and S960QL under high strain rate”, Journal of Constructional Steel Research,150, 570-580, 2018.
[16] Yang X., Yang H. and Zhang S., “Rate-dependent constitutive models of S690 high-strength structural steel”, Construction and Building Materials, 198, 597-607, 2019.

[17] Yang X., Yang H., Lai Z. and Zhang S., “Dynamic tensile behavior of S690 high-strength structural steel at intermediate strain rates”, Journal of Constructional Steel Research, 168, 105961, 2020.
[18] Chen J., Shu W. and Li J., “Experimental study on dynamic mechanical property of Q235 steel at different strain rates”, Journal of Tongji University (Natural Science) 44, 1071-1075, 2016. (In Chinese).
[19] Singh N.K., Cadoni E., Singha M.K. and Gupta N.K., “Dynamic tensile and compressive behaviors of mild steel at wide range of strain rates”, Journal of Engineering Mechanics, 139, 1197-1206, 2013.
[20] Chen J., Shu W.and Li J., “Constitutive model of Q345 steel at different intermediate strain rates”, International Journal of Steel Structures, 17, 127-137, 2017.
[21] Chen J., Li J. and Li Z., “Experiment research on rate-dependent constitutive model of Q420 steel”, Construction and Building Materials, 153, 816-823, 2017.
[22] Forni D., Chiaia B. and Cadoni E., “Strain rate behavior in tension of S355 steel: base for progressive collapse analysis”, Engineering Structures, 119, 164-173, 2016.
[23] Yang H., Yang X. and Varma A.H., “Strain-Rate effect and constitutive models for Q550 high-strength structural steel”, Journal of Materials Engineering and Performance, 28, 6626-6637, 2019.
[24] Xiong M. X., and Liew J.Y.R., “Experimental study to differentiate mechanical behaviours of TMCP and QT high strength steel at elevated temperatures”, Construction and Building Materials, 242:118105, 2020.
[25] ISO 26203-2: 2011, Metallic materials - Tensile testing at high strain rates - Part 2: Servo-hydraulic and other test systems, International Organization for Standardization (ISO/TC 164/SC 1), Switzerland, 2011.
[26] Zeng X., Huo J.S., Wang H.T., Wang Z. and Elchalakani M., “Dynamic tensile behavior of steel HRB500E reinforcing bar at low, medium, and high strain rates”, Materials. 13, 185, 2020.
[27] Zeng X., Wang Z. and Huo J.S., “Tensile behavior of 400 MPa-grade anti-earthquake hot-rolled ribbed bar (HRB400E) over a wide strain rate range”, Construction and Building Materials, 249 (2020) 118729.
[28] ASTM E8/E8M-16a, Standard Test Methods for Tension Testing of Metallic Materials, ASTM International, West Conshohocken, PA , 2016.
[29] ISO 6892-1: 2016, Metallic materials - Tensile testing - Part 1: Method of test at room temperature, International Organization for Standardization (ISO/TC 164/SC 1), Switzerland, 2016.
[30] Cowper G. and Symonds P.S., Strain hardening and strain rate effects in the impact loading of the cantilever beams - Technical Report 28, Providence, RI: Brown University, Division of Applied Mathematics, 1957.
[31] Johnson G.R. and Cook W.H., “A constitutive model and data for metals subjected to large strains, high strain rates and high temperatures”, Proceedings of the 7th International Symposium on Ballistics, 1983.
[32] Allen D.J., Rule W.K. and Jones S.E., “Optimizing material strength constants numerically extracted from taylor impact data”, Experimental Mechanics, 37, 333-338, 1997.
[33] Huh H. and Kang W.J., “Crash-worthiness assessment of thin-walled structures with the high-strength steel sheet”, International Journal of Vehicle Design, 30, 1-21, 2002.
[34] Paul S.K., “Predicting the flow behavior of metals under different strain rate and temperature through phenomenological modeling”, Computational Materials Science, 65, 91-99, 2012.
[35] Totten G.E., Xie L. and Futanani K., Modeling and simulation for material selection and mechanical design, Marcel Dekker, NewYork, 2004.